ACS Catalysis

Research Article

pubs.acs.org/acscatalysis

Ruthenium Nanoparticles Supported on Carbon: An Active Catalyst for the Hydrogenation of Lactic Acid to 1,2-Propanediol

Sarwat Iqbal,[†] Simon A. Kondrat,[†] Daniel R. Jones,[†] Daniël C. Schoenmakers,[†] Jennifer K. Edwards,[†] Li Lu,[‡] Benjamin R. Yeo,[†] Peter P. Wells,[§,⊥] Emma K. Gibson,[§,⊥] David J. Morgan,[†] Christopher J. Kiely,[‡] and Graham J. Hutchings*[,†]

[†]Cardiff Catalysis Institute, School of Chemistry, Main Building, Cardiff University, Park Place, Cardiff CF10 3AT, United Kingdom

[‡]Department of Materials Science and Engineering, Lehigh University, 5 East Packer Avenue, Bethlehem, Pennsylvania 18015-3195, United States

[§]The UK Catalysis Hub, Research Complex at Harwell, Harwell, Oxon OX11 0FA, United Kingdom

[⊥]Kathleen Lonsdale Building, Department of Chemistry, University College London, Gordon Street, London, WC1H 0AJ, United Kingdom

Supporting Information

ABSTRACT: The hydrogenation of lactic acid to form 1,2-propanediol has been investigated using Ru nanoparticles supported on carbon as a catalyst. Two series of catalysts which were prepared by wet impregnation and sol-immobilization were investigated. Their activity was contrasted with that of a standard commercial Ru/C catalyst (all catalysts comprise 5 wt % Ru). The catalyst prepared using sol-immobilization was found to be more active than the wet impregnation materials. In addition, the catalyst made by sol-immobilization was initially more active than the standard commercial catalyst. However, when reacted for an extended time or with successive reuse cycles, the sol-immobilized catalyst became less active, whereas the standard commercial catalyst became steadily more active. Furthermore, both catalysts exhibited an induction period during the first 1000 s of reaction. Detailed scanning transmission electron microscopy, X-ray photoelectron spectroscopy and X-ray absorption fine structure analysis data, when correlated with the catalytic performance results, showed that the high activity can be ascribed to highly dispersed Ru nanoparticles. Although the sol-immobilization method achieved these optimal discrete Ru nanoparticles immediately, as can be expected from this preparation methodology, the materials were unstable upon reuse. In addition, surface lactide species were detected on these particles using X-ray photoelectron spectroscopy, which could contribute to their deactivation. The commercial Ru/C catalysts, on the other hand, required treatment under reaction conditions to change from raft-like morphologies to the desired small nanoparticle morphology, during which time the catalytic performance progressively improved.

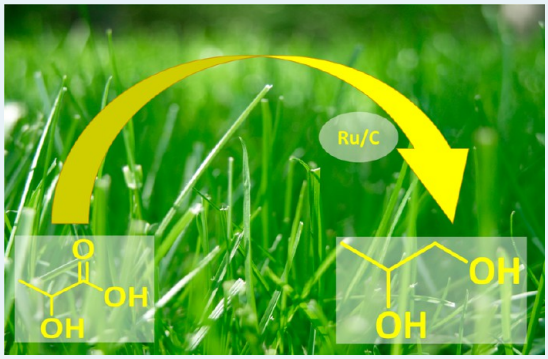

KEYWORDS: *Catalytic hydrogenation, lactic acid, Ru/C, catalyst reuse, propane diol, propylene glycol*

INTRODUCTION

1,2-Propanediol (PDO) is an attractive commodity chemical, frequently used as a deicing fluid and antifreeze as well as in the production of cosmetics and pharmaceuticals.[1] The production of PDO currently requires the selective oxidation of propene and involves environmentally unfriendly processes e.g. hydroperoxidation chemistry or the chlorohydrin process, which utilizes hypochlorous acid. PDO can also, in principle, be generated from lactic acid or lactate esters, providing an alternative and much greener production pathway than the conventional commercial synthesis. Fermentation of glucose can produce large quantities of lactic acid, and its cost is expected to decrease as advances are made in fermentation and separation techniques. Hence, lactic acid can be considered to be a platform material that is derived from biomass that can form the starting point for the manufacture of a series of derivatives. We consider that 1,2-propanediol is a viable target molecule, and if a suitable catalyst can be identified, an economically viable green route for the production of 1,2-propanediol from biomass would become available.

The catalytic hydrogenation of lactic acid to PDO requires the formation of an alcohol by the hydrogenation of a carboxyl group without removal of the α-hydroxyl group. The hydrogenolysis of the α-hydroxyl group would result in the formation of propionic acid.[2] Previous studies have indicated that relatively harsh reaction conditions are required for the hydrogenation of lactic acid and its esters, because of the intrinsically low reactivity of carboxylic acid groups with hydrogen.[3−6]

Received: March 23, 2015
Revised: July 10, 2015
Published: July 15, 2015

DOI: 10.1021/acscatal.5b00625
ACS Catal. 2015, 5, 5047−5059

Thermodynamic considerations also suggest that the formation of propionic acid is favored compared with 1,2-propanediol.[2]

Cortright et al.[7] have experimentally shown that lower temperature and higher hydrogen pressure can favor the formation of PDO from lactic acid. The first catalytic hydrogenation of lactic acid was reported by Broadbent et al.[8] over an unsupported Re black catalyst at 150 °C, and 27 MPa pressure of H_2 in which they achieved an 80% yield of PDO. Copper/chromium oxide and Raney nickel catalysts have also been reported to give yields of PDO using ethyl lactate as a substrate. The yield of PDO was as high as 80% at 250 °C and 20−30 MPa of H_2.[9]

Several recent studies have reported Ru-based catalysts as being highly active for lactic acid hydrogenation.[10−16] For instance, Zhang et al.[10] found that hydrogenation of lactic acid to PDO is possible over a Ru-containing catalyst at 150 °C and 14.5 MPa of H_2. In subsequent studies, the vapor phase hydrogenation of lactic acid was performed over a Cu/SiO_2 catalyst, which led to high conversion and good selectivity for PDO, even at atmospheric pressure.[7] In addition, $-Cu/SiO_2$,[7] Pd/SiO_2, Ni/SiO_2, and Fe/SiO_2[16] catalysts have all been shown to be efficient catalysts for this reaction, but only under relatively harsh reaction conditions. Lei et al.[17] described a novel method of lactic acid hydrogenation utilizing syngas over a Au/ZrO_2 catalyst.

Overall, however, the supported Ru-based catalysts have generated increasing attention in the literature for this reaction because of their superior intrinsic activities.[2] Ru supported on activated carbon, Al_2O_3, and TiO_2 have all been shown to be more active than Raney nickel, copper chromite, and Ni/Al_2O_3[10,18] A bifunctional Ru/TiO_2 catalyst has been proposed for this reaction at 150 °C, where the small Ru nanoparticles serve to dissociate molecular hydrogen and the TiO_2 support activates the carbonyl group.[18] There are also some reports available that describe the effects of promoters such as Sn, B, Co, Fe, and Zn on Ru-based catalysts for the hydrogenation of lactic acid.[16,17]

We consider the efficient synthesis of 1,2-propanediol from lactic acid an area of considerable interest in modern day green chemistry. To some extent, selective synthesis has already been achieved with several catalysts, including Ru-based catalysts. The Ru−C materials are the most widely studied catalysts for this reaction, but most of the literature is focused on using commercially available Ru−C materials for either (i) characterizing the reaction parameters, or (ii) for comparing different promoters. In the current study, we report that various different types of carbon can be used for supporting the Ru nanoparticles and that they show different activities under moderate reaction conditions. We also compare the activity of a sol-immobilized Ru/C catalyst with a commercial Ru−C catalyst and reconcile variations in their catalytic performance to nanostructural differences deduced using a complementary selection of advanced materials characterization techniques.

Table 1. LA Conversion and Selectivity to PDO for 5 wt % Ru Catalysts Supported on Carbon Prepared by the Wet Impregnation Method

catalyst (Ru/C)	LA conversion (%)	PDO selectivity (%)
commercial	19	100
ROX0.8	13	100
GCN3070	10	100
G60	9	100
graphene oxide	2	100
XC72R	15	100

Reaction conditions: 5 wt % LA (0.5 g) in water (9.5 g), 120 °C, 35 bar H_2, 2.5 h.

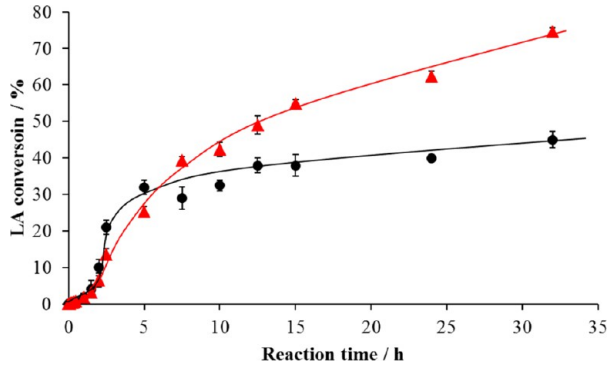

Figure 1. Effect of the reaction time on lactic acid conversion. Key: ●, 5 wt % Ru/XC72R-SI; ▲, 5 wt % Ru/C commercial catalyst. Reaction conditions: 120 °C, 35 bar H_2, 5% LA/H_2O, catalyst (0.025 g).

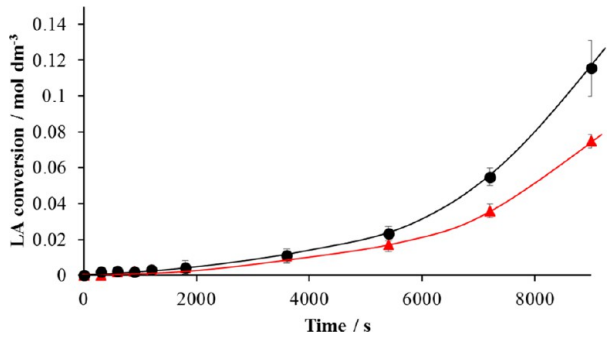

Figure 2. Effect of reaction time during the initial reaction period. Key: ▲, commercial 5 wt % Ru/C; ●, 5 wt % Ru/CXC72-SI. Reaction conditions: 120 °C, 35 bar H_2, 5% LA/H_2O, catalyst (0.025 g).

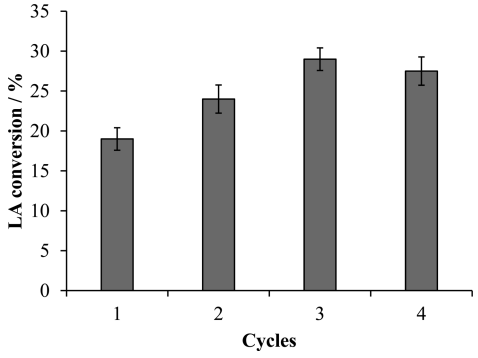

Figure 3. Effect of number reuse cycles on the LA conversion for the commercial 5 wt % Ru/C catalyst. Reaction conditions: LA (0.5 g) in water (0.95 g), 120 °C, 35 bar H_2, 2.5 h reaction time catalyst (0.025 g).

EXPERIMENTAL METHODS

Materials. A number of activated carbon supports (Darco G60, Cabot Vulcan XC72R, Norit GCN3070, and Norit ROX 0.8) were obtained for use in this study. Graphene oxide was purchased from Sigma-Aldrich. Solutions of $RuNO(NO_3)_3$ (Sigma-Aldrich, 1.5 wt % Ru) and $RuCl_3$ (Sigma-Aldrich,

DOI: 10.1021/acscatal.5b00625
ACS Catal. 2015, 5, 5047−5059

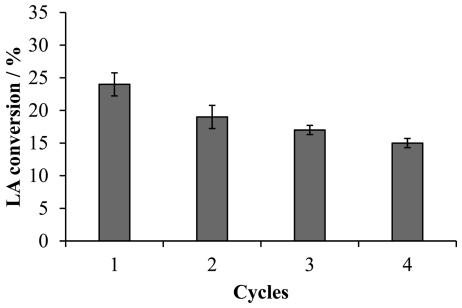

Figure 4. Effect of number of reuse cycles on the LA conversion for the 5 wt % Ru/C XC72R-SI catalyst. Reaction conditions: LA (0.5 g) in water (0.95 g), 120 °C, 35 bar H_2, 2.5 h reaction time, catalyst (0.025 g).

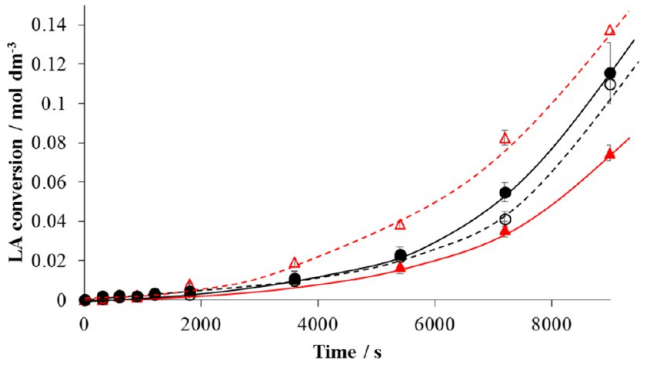

Figure 5. Effect of the reaction time during the initial reaction period. Key: ▲, commercial 5 wt % Ru/C fresh; ●, 5 wt % Ru/CXC72-SI fresh; Δ, commercial 5 wt % Ru/C after one use; ○, 5 wt % Ru/CXC72-SI after one use. Reaction conditions: 120 °C, 35 bar H_2, 5% LA/H_2O, catalyst (0.025 g).

45−55 wt % Ru) were used as ruthenium precursors. Lactic acid (Sigma-Aldrich, 98%) was used as received. Possible liquid products (1,2-propanediol, propionic acid, methanol, ethanol, 1-propanol, and 2-propanol) were purchased from Sigma-Aldrich, and possible gas products (methane, ethane, and propane) were purchased from BOC. These were used as standards for calibration and determination of analytical purity. A commercial 5 wt % Ru/C (Sigma-Aldrich) catalyst was used as a baseline to compare the activity of the synthesized catalysts.

Catalyst Preparation. Catalysts were prepared by two methods: namely, wet impregnation (WI) and sol immobilization (SI). For WI catalysts, a solution of $RuNO(NO_3)_3$ (5 wt % with respect to activated carbon) was added to the support to obtain a paste. The catalyst was then dried (110 °C, 16 h) and subsequently heat-treated in N_2 (400 °C, 3 h, 20 °C/min ramp rate). SI catalysts were prepared starting from a solution of PVA (10 mg) and $RuCl_3$ (0.04 g) in water (800 mL). A freshly prepared solution of $NaBH_4$ ($RuCl_3/NaBH_4$ = 1/3.3 mol %) was then added to generate the sol. After 30 min, the activated carbon (1.98g) was added, and the solution was acidified to pH 2 with sulfuric acid. The catalyst was then filtered and dried (110 °C, 16 h).

Catalyst Characterization. X-ray powder diffraction (XRPD) was performed using a PANalytical X'Pert Pro diffractometer fitted with an X'Celerator detector and a Cu Kα X-ray source operated at 40 kV and 40 mA. Temperature-programmed reduction (TPR) analysis was performed with a Quantachrome ChemBet system equipped with a cold trap using 10% H_2/Ar (5 mL/min) and a ramp rate of 20 °C/min. Samples (0.5 g)

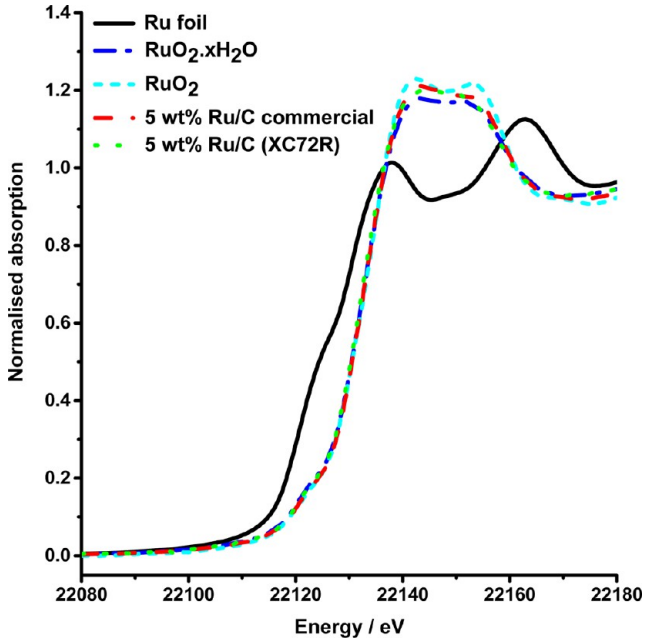

Figure 6. Normalized XANES spectra for (i) the standard commercial 5 wt % Ru/C catalyst, (ii) the most active 5 wt % Ru/C XC72R-SI catalyst, (iii) $RuO_2{\cdot}xH_2O$, (iv) anhydrous RuO_2 and (v) metallic Ru foil. The inset figure shows the expanded XANES region for these materials.

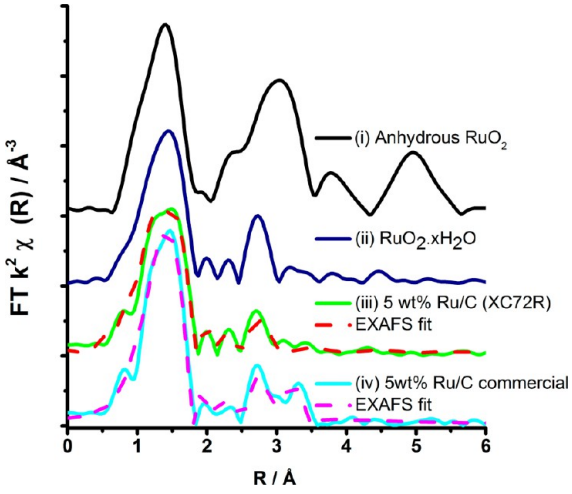

Figure 7. Fourier Transform of the χ^2-weighted EXAFS spectra of (i) anhydrous RuO_2, (ii) $RuO_2{\cdot}xH_2O$, (iii) the 5 wt % Ru/C commercial catalyst, and (iv) 5 wt % Ru/C XC72R-SI catalyst. Simulated EXAFS fits are also shown as red and purple dashed lines for the two Ru/C catalyst samples.

were pretreated at 100 °C (ramp rate, 20 °C/min) under He for 1 h prior to analysis.

Samples for examination by scanning transmission electron microscopy (STEM) were prepared by dispersing the dry catalyst powder onto a holey carbon film supported by a 300 mesh copper TEM grid. Samples were then subjected to bright field (BF) and high-angle annular dark field (HAADF) imaging using an aberration-corrected JEOL ARM 200CF microscope operating at 200 kV.

Microwave plasma atomic emission spectroscopy (MP−AES) was performed using an Agilent 4100 MP−AES. The Ru content was analyzed with two emission lines at 349.894 and

DOI: 10.1021/acscatal.5b00625
ACS Catal. 2015, 5, 5047−5059

Table 2. EXAFS Fitting Parameters for the Standard Commercial 5 wt % Ru/C Catalyst and the 5 wt % Ru/XC72R_SI Catalyst Shown in Figure 6

sample	Abs Sc	N	R, Å	$2\sigma^2$, Å^2	E_0, eV	R_{factor}
5 wt % Ru/XC72R-SI catalyst	Ru−O	1.8 (4)	1.85 (2)	0.008 (1)	−5 (1)	0.02
	Ru−O	3.7(4)	2.02 (1)	0.012 (5)		
	Ru−Ru	2.0 (6)	3.12 (1)	0.009(2)		
5 wt % Ru/C commercial catalyst	Ru−O	1.9 (4)	1.87 (2)	0.003 (2)	−4 (2)	0.04
	Ru−O	4.0 (5)	2.00 (1)	0.003 (1)		
	Ru−Ru	2.2 (6)	3.11 (2)	0.008 (2)		
	Ru−Ru	2.0 (6)	3.56 (2)	0.006 (1)		

Fitting parameters: S_0^2 = 0.85 as deduced from a Ru foil standard; fit range 2.5 < k < 14, 1 < R < 4; number of independent points = 22.

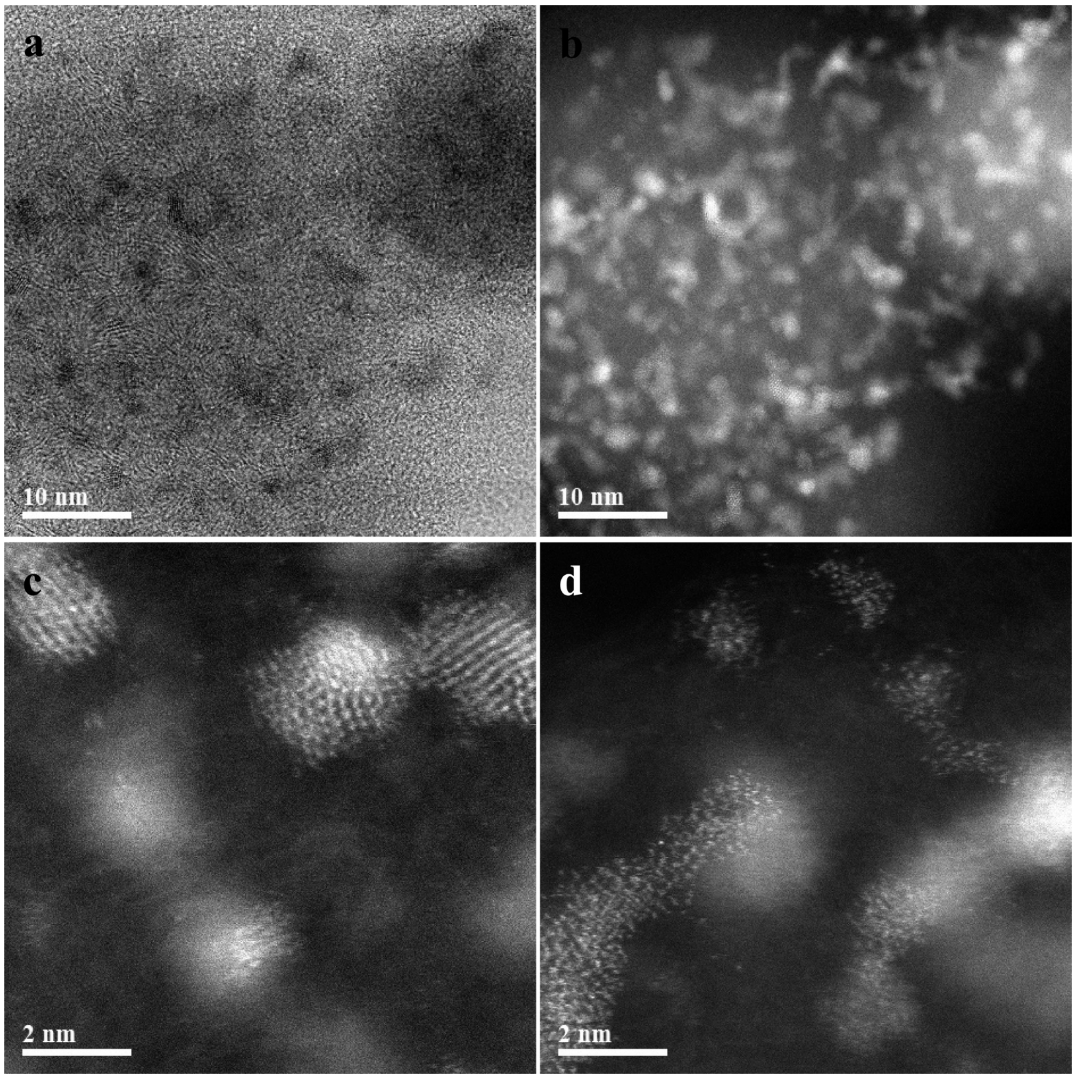

Figure 8. Low-magnification (a) BF-STEM and (b) HAADF-STEM images showing the typical particle size and shape distribution in the unused commercial Ru/C catalyst and (c, d) higher-magnification HAADF images showing greater structural detail in individual particles.

371.803 nm. The samples were introduced to the nitrogen plasma using a single pass spray chamber at a pressure of 120 kPa without air injection. The instrument was calibrated with 1, 2, 4, 7, and 10 ppm standards in 10% HCl along with a 5% lactic acid blank. The samples were tested in triplicate, and the average result was used. A lactic acid rinse solution (5%) was introduced between samples for 15 s to ensure there was no sample contamination.

Samples were characterized by X-ray photoelectron spectroscopy (XPS) using a Kratos Axis Ultra-DLD photoelectron spectrometer, utilizing monochromatic Al Kα radiation. High-resolution and survey scans were performed at pass energies of 40 and 160 eV, respectively. Spectra were calibrated to the C(1s) signal at 284.5 eV.

Surface area and pore size analysis were determined by N_2 adsorption at 77 K using a Quantachrome Autosorb AS1 system. Samples were degassed for a minimum of 24 h at 120 °C before the analysis. Surface areas were evaluated using the BET method, and the pore size distribution was determined by

DOI: 10.1021/acscatal.5b00625
ACS Catal. 2015, 5, 5047−5059

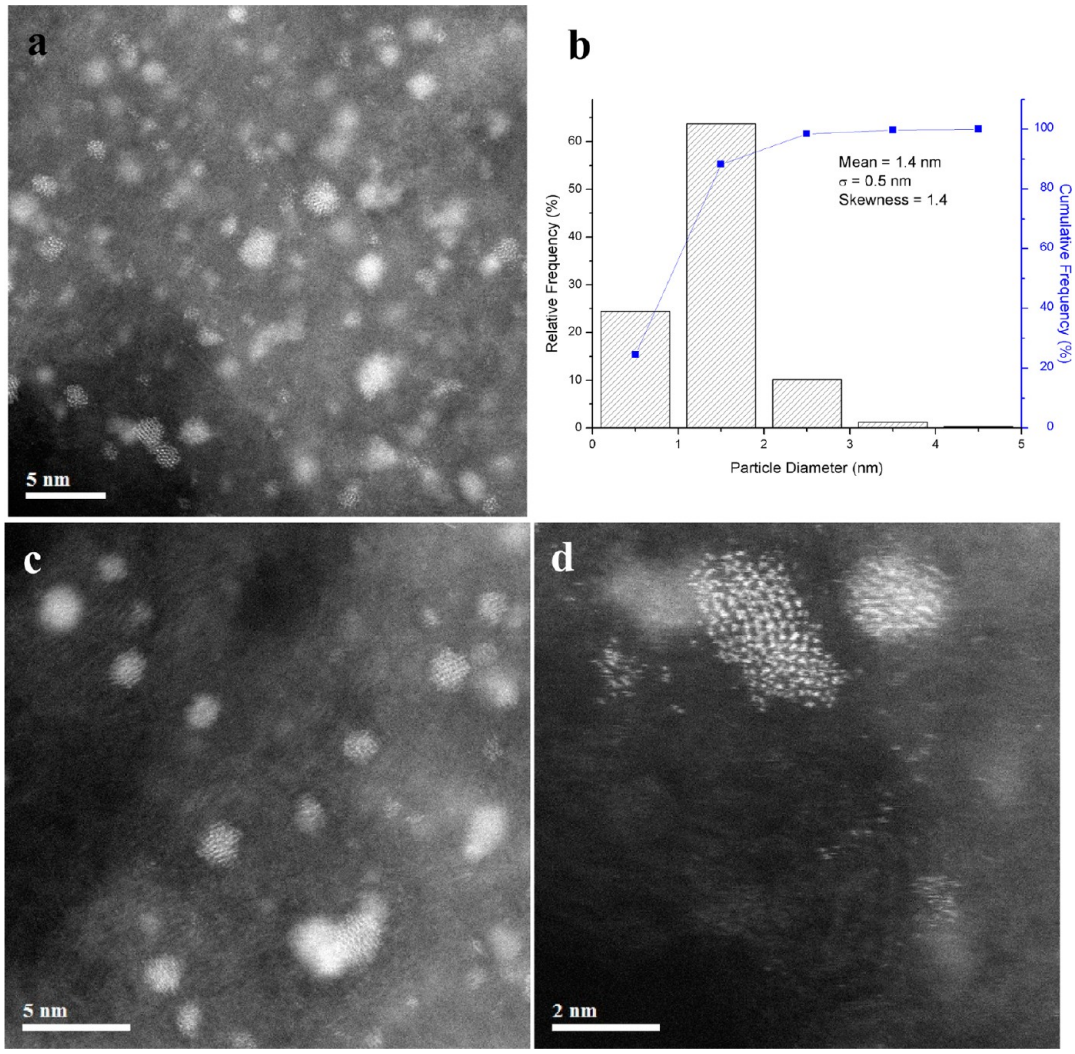

Figure 9. (a) Low-magnification HAADF-STEM image, (b) the corresponding particle size distribution from the commercial Ru/C catalyst used once, and (c, d) higher-magnification HAADF images showing greater structural detail in individual particles.

applying the nonlocal density functional theory (NLDFT) method.

Ru K edge XAFS studies were carried out on the B18 beamline at the Diamond Light Source, Didcot, U.K. Measurements were performed using a QEXAFS setup with a fast-scanning Si (311) double crystal monochromator. The time resolution of the spectra reported herein was 5 min/spectrum (k_{max} = 14, step size 0.5 eV). On average, three scans were acquired to improve the signal-to-noise level of the data for transmission measurements. All solid reference samples were diluted with cellulose and pressed into pellets to optimize the effective edge-step of the XAFS data and measured in transmission mode using ion chamber detectors. All XAFS spectra were acquired concurrently with the appropriate foil placed between I_t and I_{ref}. XAFS data processing was performed using IFEFFIT[19] with the Horae package[20] (i.e., Athena and Artemis methods). The amplitude reduction factor, S_0^2, was derived from EXAFS data analysis of a known reference compound, namely, Ru metal foil, which was determined to be 0.85 and used as a fixed input parameter.

Lactic Acid Hydrogenation. The hydrogenation of lactic acid was carried out using a stainless steel stirred autoclave (50 mL, Parr Instruments, model 5500HP) equipped with a Teflon liner using catalyst (0.025 g), lactic acid (0.50 g) and deionized water (9.50 g). The sealed autoclave was purged three times with N_2, and three times with H_2 before being pressurized to 35 bar with H_2. The autoclave was heated to 120 °C and stirred at 2000 rpm When the reaction was completed, the mixture was cooled and filtered, and the products were analyzed using an HPLC column (Agilent Technologies 1260 Infinity) equipped with a Varian MetaCarb 67H capillary column (0.65 × 30 cm) and a refractive index detector. Gas analysis was carried out using a gas chromatograph (Varian 450-GC) equipped with flame ionization and thermal conductivity detectors, a methaniser, and a CP-SiL5CB column (50m, 0.33 mm) using He as the carrier gas.

All the experiments were performed at least three times, and the catalytic results were compared using the standard deviation formula. These results are provided in terms of error bars.

RESULTS AND DISCUSSION

Lactic Acid Hydrogenation. Lactic acid (LA) hydrogenation was investigated over a series of 5 wt % Ru/C catalysts prepared using wet impregnation with a range of different carbon supports. The activity was compared with that of a commercial 5 wt % Ru/C catalyst that was used as a standard for this study. The results are shown in Table 1, and the only

DOI: 10.1021/acscatal.5b00625
ACS Catal. 2015, 5, 5047−5059

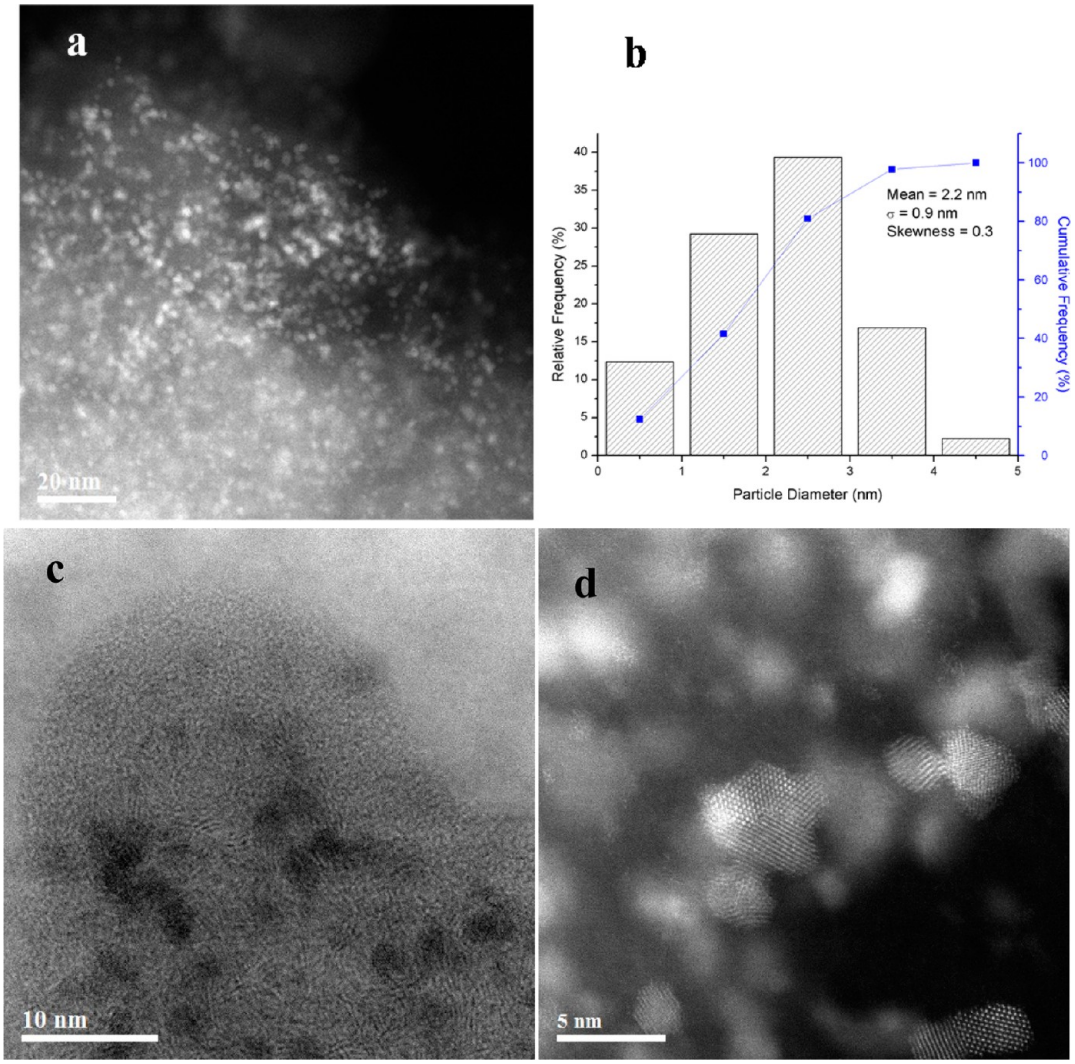

Figure 10. (a) Low-magnification HAADF-STEM image; (b) the corresponding particle size distribution from the commercial Ru/C catalyst used four times; and (c, d) higher-magnification BF and HAADF images, respectively, showing greater structural detail in individual particles.

product observed for all catalysts was PDO at the reaction temperature we studied of 120 °C. This is an interesting observation and contrasts with previous observations for this reaction.[7,21] In other studies, a number of byproducts have been observed, such as propanol, and propionic acid with Cu/SiO_2 catalysts[7] and lower hydrocarbons with Ru/C catalyst under harsher reaction conditions (e.g., high pressure).[21] However, using our Ru catalysts, we have not observed any product other than propylene glycol. This we consider is due to the different preparation method, carbon types, and reaction conditions we have utilized.

All the catalysts prepared by wet impregnation were active for the lactic acid hydrogenation reaction, but all were considerably less active than the commercial standard catalyst. Graphene oxide was found to be the least suitable support of all those tested because it exhibited a conversion of only 2%; however, the catalyst prepared using XC72R carbon as the support gave the best results, so this was selected for use as a support to investigate an alternative method of metal deposition. A 5 wt % Ru on XC72R carbon catalyst was prepared using sol-immobilization (designated Ru/C XC72R-SI). When investigated for lactic acid hydrogenation, this sol-immobilized material was more active than the commercial 5 wt % Ru/C standard catalyst. It was also more active than the Ru/C XC72R prepared by the wet impregnation method, showing that the type of carbon as well as the Ru deposition method have a significant effect on the catalytic activity. Using reaction conditions that were the same as those used for the wet impregnation catalysts, the Ru/C XC72R-SI catalyst gave 23% conversion, compared with 19% for the commercial catalyst (Table 1) after 2.5 h of reaction. Again, only PDO was observed as a product.

We decided to investigate the Ru/C XC72R-SI and commercial catalysts in more detail. Figure 1 shows the effect of the reaction time on the LA conversion. PDO was the only product for the reactions performed over longer reaction times. No byproducts were detected in either liquid or gas phases. It is apparent that there are three features characteristic of the reaction profile. First, there is an induction period for both catalysts; second, the catalyst prepared by sol-immobilization is initially more active than the commercial Ru catalyst, and subsequently, the sol-immobilized catalyst becomes deactivated, but the commercial Ru catalyst retains activity and after 5 h of reaction demonstrates higher activity.

The induction period of ~1000 s is observed for both catalysts, and Figure 2 shows this more clearly. There are several

DOI: 10.1021/acscatal.5b00625
ACS Catal. 2015, 5, 5047−5059

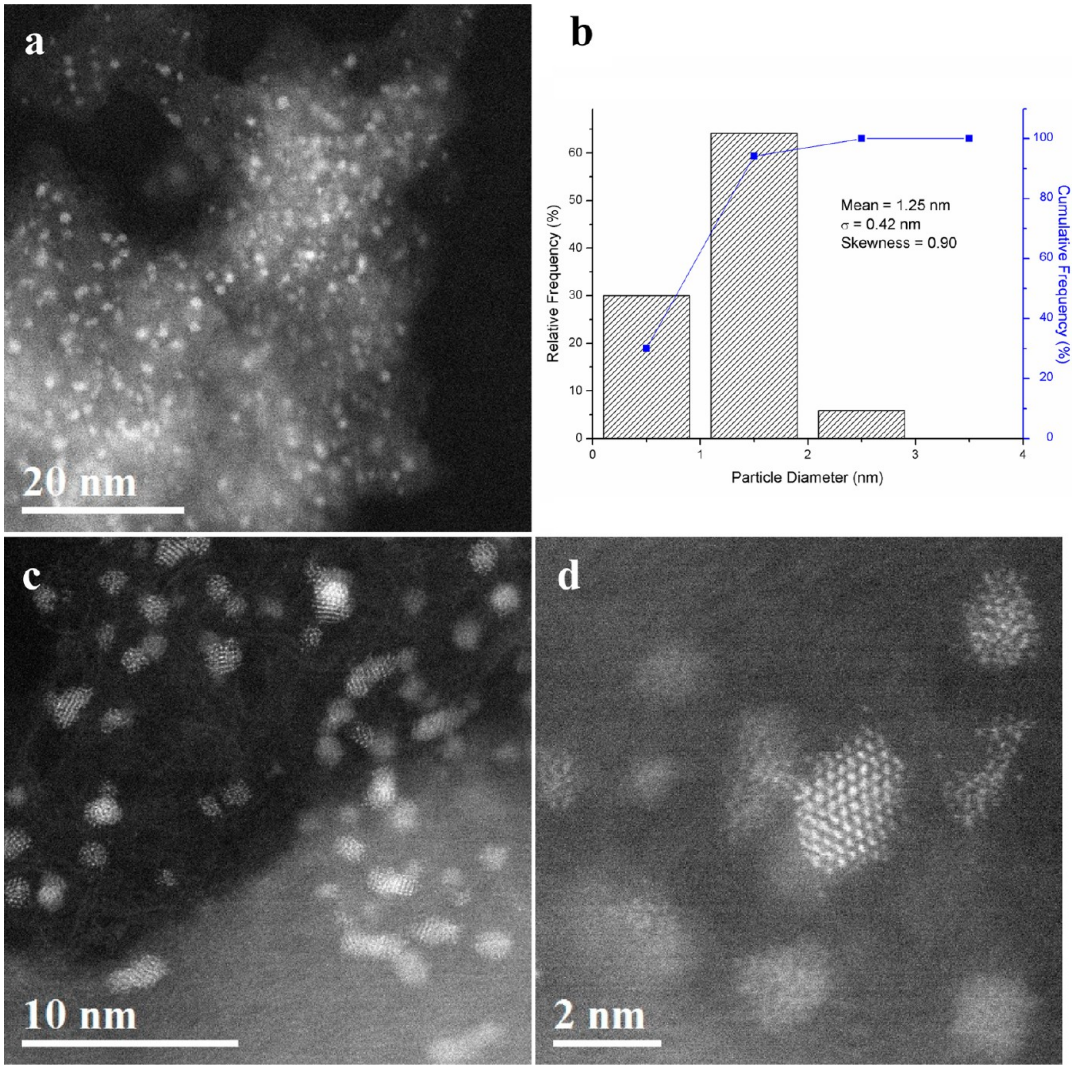

Figure 11. (a) Low-magnification HAADF-STEM image, (b) the corresponding particle size distribution from the unused sol immobilized Ru/C XC72R catalyst, and (c, d) higher-magnification HAADF images showing greater structural detail in individual particles.

reasons why an induction period may be observed. First, it is possible that Ru is leached from the catalyst, and homogeneous catalysis then ensues. Reaction mixtures were analyzed for Ru by MP−AES, and no leaching was detected. Hence, any changes in the reaction rate cannot be attributed to loss of Ru from the catalyst or due to a homogeneous reaction. Second, the effect could be due to the initial reduction of the catalyst. To investigate this, we prereduced both catalysts (5 wt % Ru/CXC72-SI and 5 wt % Ru/C commercial) in H_2 ex situ; however, these catalysts were less active than the nonreduced catalysts (after 2.5 h: 23% LA conversion for the nonreduced versus 18% LA conversion for the prereduced 5 wt % Ru/CXC72-SI catalyst and 19% LA conversion for the nonreduced versus 13% LA conversion for the prereduced 5 wt % Ru/C commercial). The induction period may therefore involve the creation of the active surface, which involves the presence of LA and H_2.

Following the induction period and between 1000 and 9000 s, the reaction is first-order in LA with the measured first order rate constants being 4.5×10^{-4} s^{-1} (for 5 wt % Ru/CXC72-SI) and 3.7×10^{-4} s^{-1} (for the commercial 5 wt % Ru/C catalyst). The turnover frequencies (TOFs) were calculated, and the data provided in the literature[10,22] was used to calculate the TOF for a comparison purpose. For the 5 wt % Ru/CXC72-SI, the TOF is 4116 h^{-1} (productivity = 1.84 mol LA $g_{catalyst}^{-1}$ h^{-1}), compared with 2312 h^{-1} (productivity = 1.1 mol LA $g_{catalyst}^{-1}$ h^{-1}) for the commercial catalyst. These values for our Ru catalysts are far higher than that reported by Miller et al.,[10] 405 h^{-1} (productivity = 0.20 mol LA $g_{catalyst}^{-1}$ h^{-1}), and Jang et al.,[22] 1435 h^{-1} (productivity = 0.71 mol LA $g_{catalyst}^{-1}$ h^{-1}), who also used a 5% Ru/C catalyst together with more severe reaction conditions (150 °C and 50 bar H_2).

An important feature of any catalyst performance is that it should be reusable. In view of this, we have conducted a series of reusability experiments using the same catalyst mass in each experiment. The catalysts were used for 2.5 h then recovered, washed with water, dried, and then reused. The results for the commercial 5 wt % Ru/C catalyst are shown in Figure 3 for four successive reuse cycles.

An increase in conversion occurs with successive catalyst reuse cycles. PDO was the only product detected in all these experiments. We then conducted reuse experiments for the 5 wt % Ru/C XC72R-SI material, which showed a distinctly different reuse profile with a steady decrease in activity being observed on each subsequent reuse, again with PDO being the only product detected (Figure 4). These trends are in direct agreement with the reaction profile noted in Figure 1 because the four successive reuses simulate the reaction over the first

DOI: 10.1021/acscatal.5b00625
ACS Catal. 2015, 5, 5047−5059

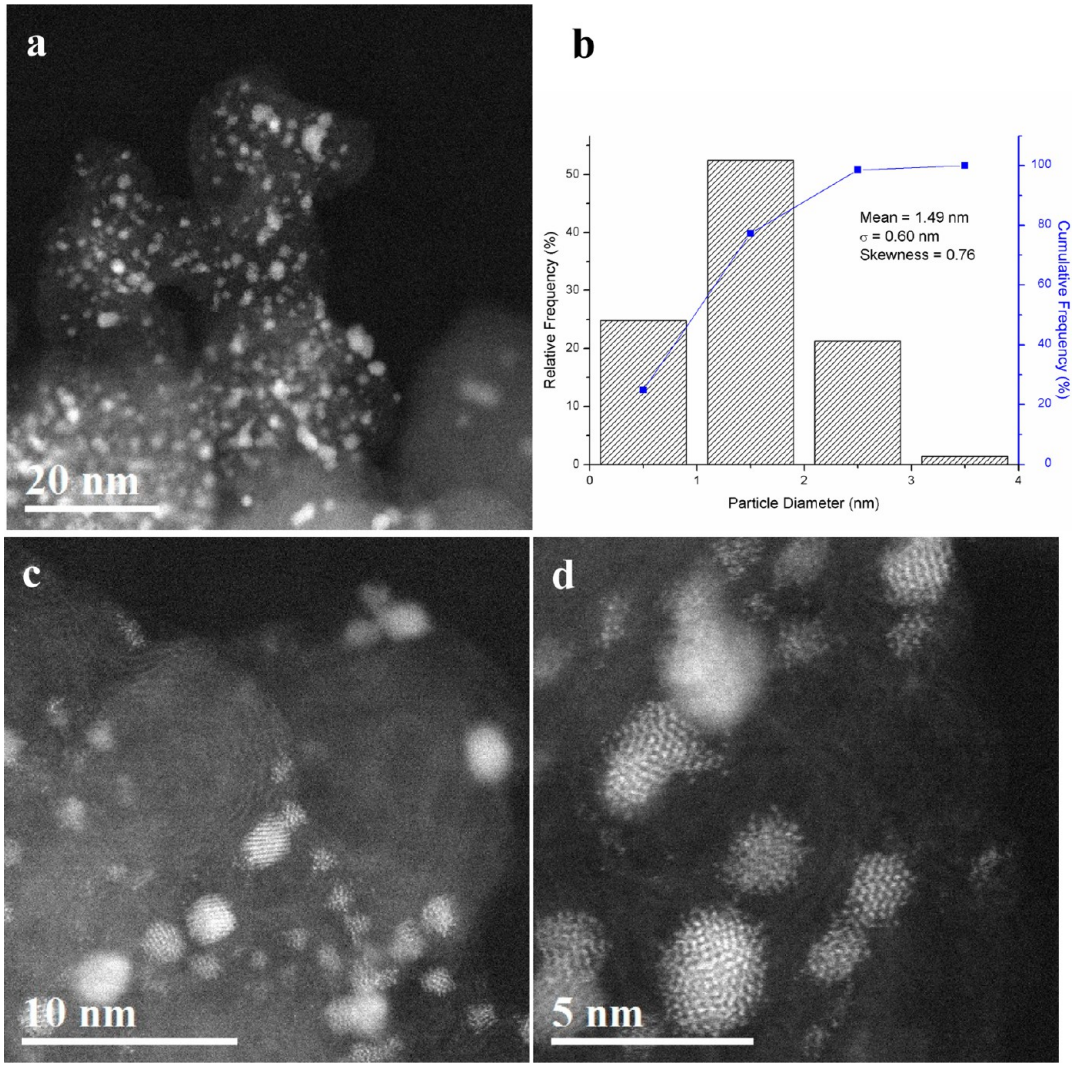

Figure 12. (a) Low-magnification HAADF-STEM image, (b) the corresponding particle size distribution from the sol-immobilized Ru/C XC72R-SI catalyst used once, and (c, d) higher-magnification HAADF images showing greater structural detail in individual particles.

10 h reaction period. For the commercial catalyst during this reaction time, the activity increases, whereas the sol-immobilized catalyst initially has a higher activity that then declines. Further, we studied the time on line effect on both catalysts after their first use; the data are presented in Figure 5. Interestingly, no change in induction period was observed for 1000 s with both of the used catalysts. A comparison of the time online data of the used catalysts with the fresh catalysts showed that there is an increase in catalytic activity of the used commercial 5 wt % Ru/C catalyst after ~3600 s, and the activity of the Ru/C XC72R-SI catalyst remained similar to the fresh catalyst. This trend is further observed in the successive reuse cycles (Figures 3 and 4), in which the commercial 5 wt % Ru/C catalyst showed an improved activity, and a decline in activity of the Ru/C XC72R-SI catalyst was observed. To understand these effects observed in the catalytic hydrogenation reaction, we have characterized both catalysts in considerable detail.

Catalyst Characterization. The BET surface areas of the bare carbon supports and the Ru/C samples were determined along with the pore size distributions of the two most active catalysts. The data (see the Supporting Information, Tables S1, S2, and S3 and Figures S1, S2, and S3) show that the addition of Ru did not affect the overall surface area for any particular carbon support. Furthermore, although there are significant variations in surface areas and pore size distributions between the different carbons tested, there is no correlation with the observed catalyst activity. XRD patterns for the Ru catalysts supported on various carbons did not show any reflections that could be assigned to Ru (see the Figure S4), suggesting that the supported particles are smaller than 3−4 nm in size. However, the Ru surface area as determined by CO chemisorption for commercial 5 wt % Ru/C catalyst and the 5 wt % Ru/CXC72-SI sample were found to be similar (3 m^2 g^{-1}).

The 5 wt % Ru catalysts on different carbon supports were analyzed using TPR (see the Figures S6, S7). The commercial catalyst, and Ru supported on GCN3070 show two distinct reduction peaks: one below 100 °C and the other above 200 °C. The catalysts prepared by wet impregnation and sol-immobilization methods using XC72 carbon show two reduction peaks below 100 °C, whereas the catalyst prepared by the sol-immobilization method has an additional broad peak at 140 °C. The first reduction peaks at a lower temperature can be assigned to the reduction of Ru^{3+} to Ru^{2+}, and the other peak at higher temperature could be due to second-step reduction of Ru^{2+} to Ru^{1+}; however, there is also the possibility of

DOI: 10.1021/acscatal.5b00625
ACS Catal. 2015, 5, 5047−5059

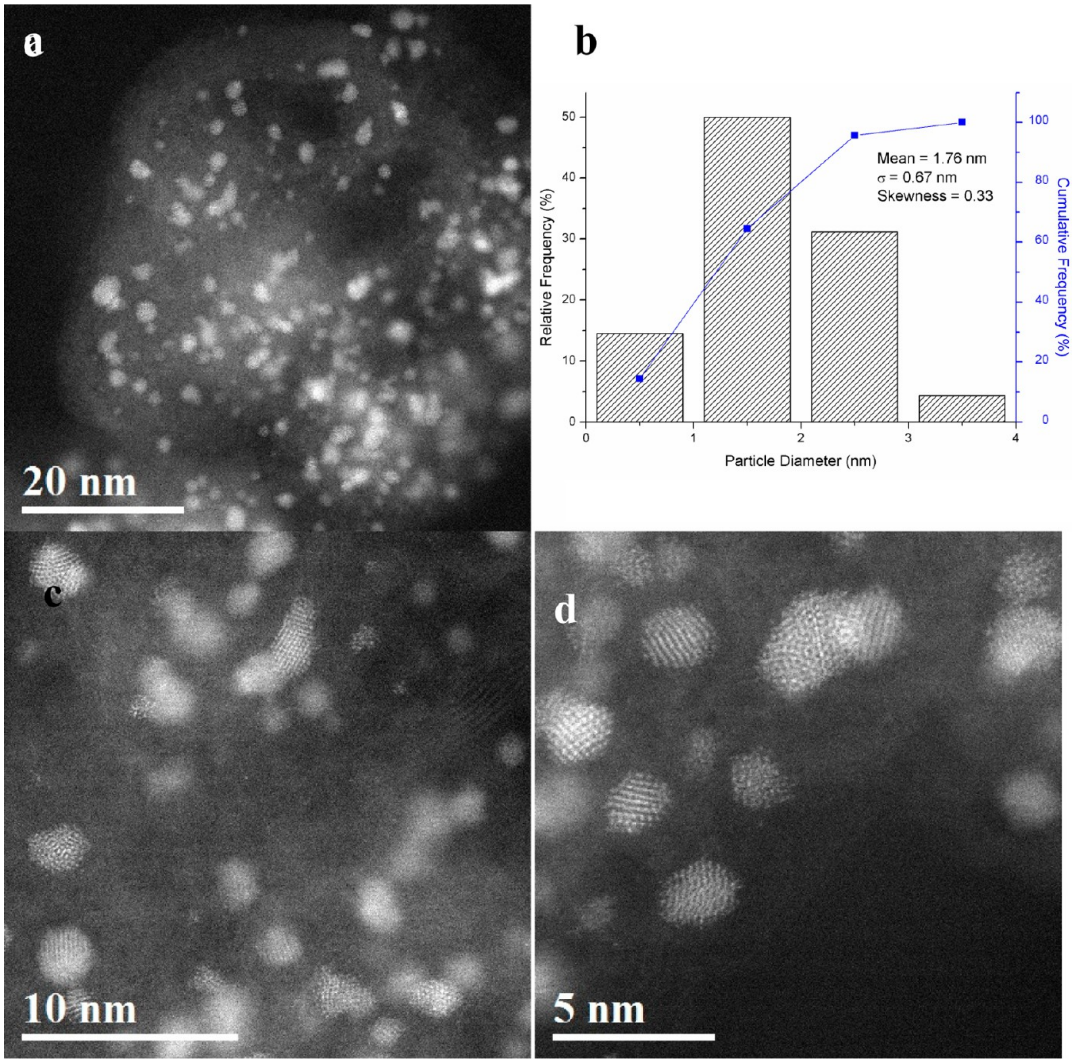

Figure 13. (a) Low-magnification HAADF-STEM image, (b) the corresponding particle size distribution from the sol-immobilized Ru/C XC72R-SI catalyst used three times, and (c, d) higher-magnification HAADF images showing greater structural detail in individual particles.

reduction of Ru^{2+} to the metallic state.[23,24] Ru supported on G60 and ROX 0.8 shows only one reduction peak just below 100 °C, but these catalysts are less active. In comparison, the graphene oxide-supported Ru catalyst exhibits a higher reduction temperature (~150 °C). None of the catalysts were reduced prior to our catalytic testing experiments; hence, we expect that all the catalysts, apart from the one supported on graphene oxide, will be reduced during the initial phase of the reaction, which takes place at 120 °C under 35 bar of H_2. This may account for the abnormally low catalytic activity exhibited by the graphene oxide-supported Ru catalyst where the lactic acid hydrogenation temperature is always kept below the 150 °C value needed for Ru reduction on the GO surface.

We decided to examine the structure of the most active sol-immobilized catalyst (Ru/C XC72R-SI) and the standard commercial catalyst using X-ray absorption fine structure (XAFS). This is a powerful technique for determining the local structure for materials such as nanoparticles that do not display long-range order, with the near-edge structure (XANES) also providing information on the oxidation state. Figure 6 shows the XANES data for the commercial 5 wt % Ru/C and 5 wt % Ru/C XC72R-SI catalysts, alongside reference spectra taken from $RuO_2{\cdot}xH_2O$, anhydrous RuO_2, and Ru metal foil. The Ru/C catalyst samples have an edge position of 22130 eV, as do both the standard ruthenium oxide samples, that is higher in energy than the edge position of the Ru foil at 22117 eV, as would be expected for a shift of the valence state from Ru^0 to Ru^{4+}. Other groups have reported the same edge position (i.e., 22130 eV) for anhydrous RuO_2 and $RuO_2{\cdot}xH_2O$, even though some Ru^{3+} centers are known to be present in the hydrated sample.[25] As such, we can also not rule out the presence of a small Ru^{3+} component in addition to Ru^{4+} in our Ru/C catalyst materials. The double maxima feature observed beyond the absorption edge is associated with anhydrous forms of RuO_2, with completely hydrated forms having only one maximum.[26] The XANES spectra of $RuO_2{\cdot}xH_2O$, the 5 wt % Ru/C commercial catalyst, and 5 wt % Ru/C XC72R-SI catalyst show varying degrees of hydration, with the 5 wt % Ru/C commercial catalyst showing the most pronounced double maxima feature, implying that it therefore has the greatest anhydrous character.

The Fourier transform of the χ^2-weighted extended X-ray absorption fine structure (EXAFS) spectra of anhydrous RuO_2, $RuO_2{\cdot}xH_2O$, the 5 wt % Ru/C commercial catalyst, and the 5 wt % Ru/C XC72R-SI catalysts are shown in Figure 7. The simulated EXAFS fits are also shown superimposed for the two

DOI: 10.1021/acscatal.5b00625
ACS Catal. 2015, 5, 5047−5059

Ru/C catalyst samples. By studying the EXAFS data, it is possible to differentiate between hydrated forms of RuO_2. When RuO_2 is hydrated, its native rutile structure is disturbed, which disrupts the Ru−Ru scattering paths in the EXAFS Fourier transform. This phenomenon has been attributed to chains of RuO_6 octahedra in which the three-dimensional network of these chains does not extend out as far as for anhydrous RuO_2.[25] This effect can be seen by the lack of features after 3 Å for the $RuO_2{\cdot}xH_2O$ sample in the Fourier transform data shown in Figure 7. The EXAFS fitting parameters (Table 2) for the two Ru/C catalyst samples show that the standard commercial material is less hydrated than the sol-immobilized Ru/C-XC72R-SI material. This is evidenced by the presence of an additional Ru−Ru coordination shell at 3.56 Å for the former catalyst, with both samples exhibiting an initial Ru−Ru distance at 3.11 Å. Both the 3.11 and 3.56 Å distances are characteristic of plane spacings present in the rutile structure expected of anhydrous RuO_2. It can therefore be deduced that the chains of RuO_6 octahedra have a more extended three-dimensional structure in the commercial Ru/C sample, although not quite as extended as that for purely anhydrous RuO_2. We therefore consider that the differences in the initial activities we observe with these two Ru/C catalysts might be associated with their different initial levels of hydration.

Because the two catalysts showed intriguingly different reaction profiles either in continuous use (Figures 1 and 2) or on successive reuse cycles (Figures 3 and 4), we subjected them to detailed characterization. No discernible change in surface area from BET analysis was observed, indicating that no significant coking that blocked access to the Ru particles was occurring. In addition, MP−AES of the reaction effluents revealed no Ru leaching. STEM analysis was performed for the fresh and used batches of both catalysts (commercial Ru/C and Ru/CXC72R-SI). Figure 8a,b shows a complementary pair of BF- and HAADF-STEM images of the unused commercial Ru/C catalyst material. It is clear that there are discrete ∼2 nm particles present as well as elongated lines, ∼1.0−1.5 nm in width and up to 10 nm in length, of Ru-containing material. These two morphologies are more clearly visible at a higher magnification in Figure 8c,d, respectively. The discrete particles are seen to be semicrystalline, whereas the raft-like structures are fairly disordered in nature and may be indicative of partially converted Ru precursor material or hydrated RuO_x. After the first use of the catalyst (see Figure 9a), the ∼2 nm particles remain, but the flat raft linear structures appear to have broken up into a population of ∼1 nm particles. The mean size of this new overall particle distribution is 1.4 nm, as illustrated in Figure 9b). Higher-magnification micrographs of these particles (Figure 9c,d) shows them to be poorly crystalline in character, suggesting they are RuO_x. After four usage cycles, the particle structure in this commercial catalyst shows further modification, as illustrated in Figure 10, with the mean particle size increasing to 2.2 nm and a considerably broader size distribution being evident (Figure 10b). High-magnification HAADF-STEM imaging also indicated (Figure 10d) that these particles are now more crystalline in nature, exhibiting interplanar spacings and angles that are more consistent with metallic Ru.

The Ru/C XC72R-SI catalyst series prepared by sol-immobilization display some marked differences to the commercial Ru/C materials when examined by STEM. As shown in Figure 11a,c,d, the unused Ru/C XC72R-SI catalyst material shows only a homogeneous dispersion of crystalline Ru-containing

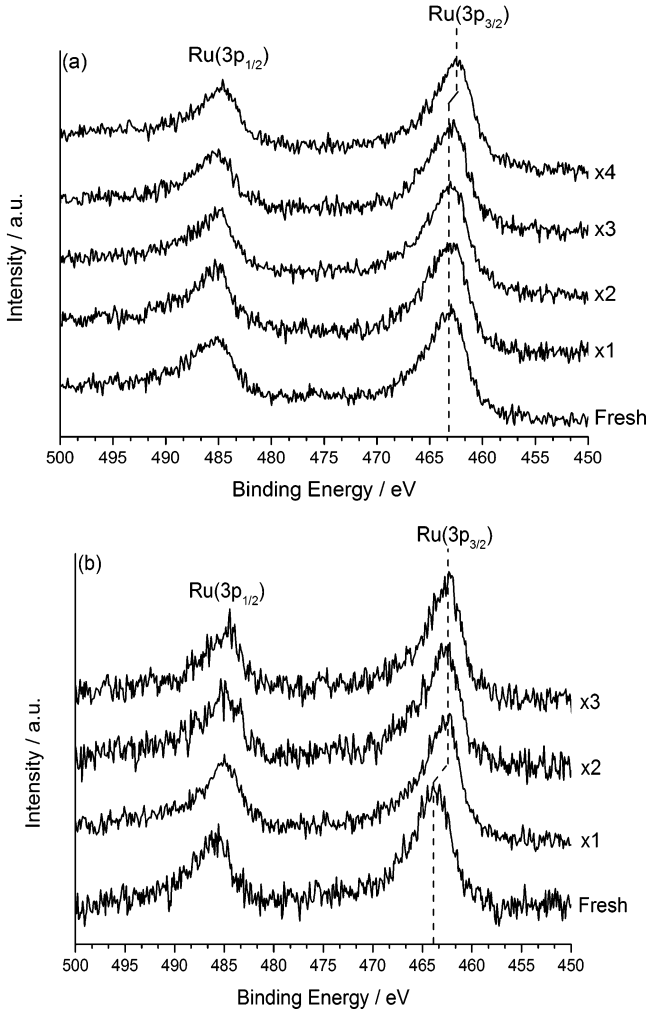

Figure 14. Ru(3p) core-level spectra for (a) the commercial 5 wt % Ru/C sample and (b) sol-immobilized 5 wt % Ru/C XC72R-SI sample after successive usage cycles.

nanoparticles from the outset. These have a mean size of 1.25 nm and a rather narrow size distribution (Figure 11b). After just one usage cycle, there is some evidence of limited particle sintering as the mean size increases slightly to ∼1.5 nm (see Figure 12a,b). In addition, many of the larger particles seem to be crystalline Ru, whereas the smaller ones appear to be more disordered and RuO_x-like in character (see Figure 12c,d). After the Ru/C XC72R catalyst had been used three times (Figure 13a,b), the gradual increase in the mean particle size due to sintering was seen to continue, reaching a value of ∼1.8 nm, and the crystallinity of the particles was largely retained (Figure 13c,d).

XPS analysis of the Ru/C catalyst systems is inherently difficult because of the overlap of the C(1s) and Ru(3d) core-levels and the asymmetric nature of the Ru core level line shape; however, chemical state information may still be obtained from observing a combination of both the Ru(3d) and the lesser-studied Ru(3p) core levels. Figures 14 and 15 show the Ru(3p) and C(1s)/Ru(3d) core-level spectra, respectively, for both the commercial and 5% Ru/C catalysts prepared by sol-immobilization using the XC72R carbon as support. For the used catalysts, there is a clear shift in the binding energies for both Ru(3p) and Ru(3d) toward lower energy. For the both commercial and sol-immobilized catalysts, the Ru(3p) energies

DOI: 10.1021/acscatal.5b00625
ACS Catal. 2015, 5, 5047−5059

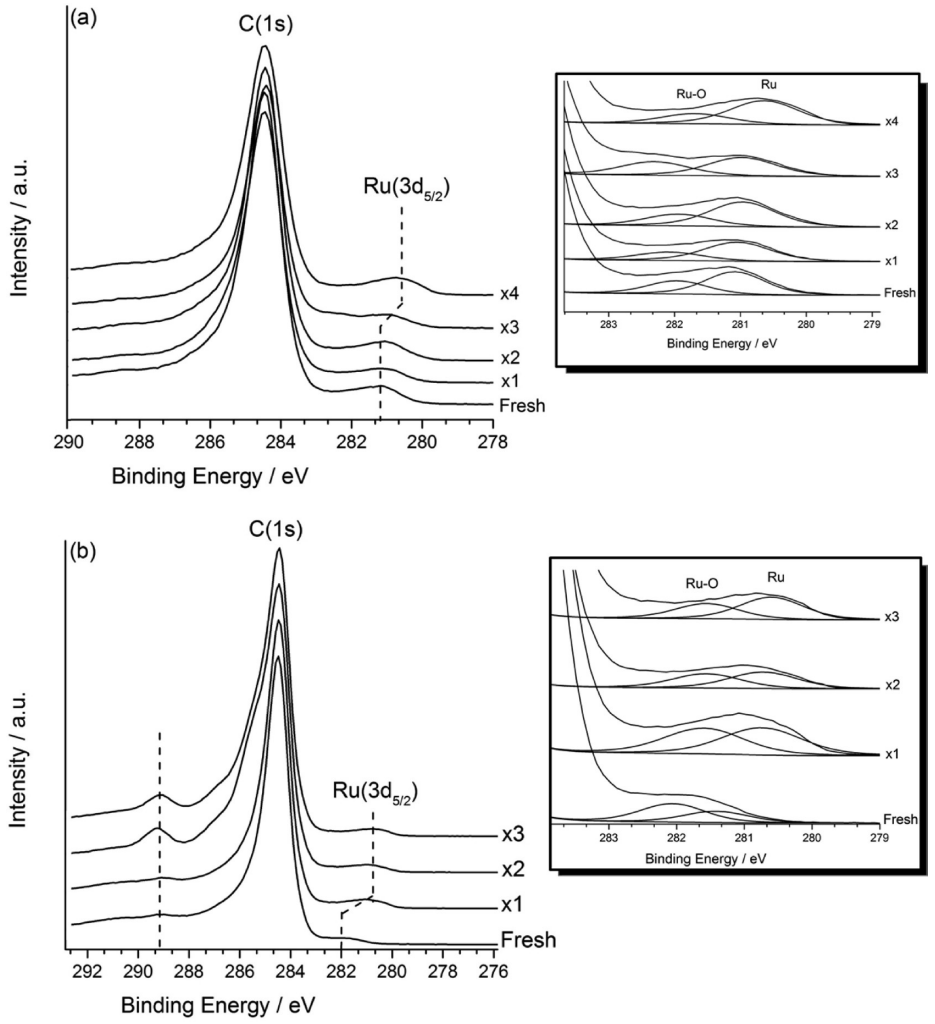

Figure 15. C(1s)/Ru(3d) core-level spectra for (a) the commercial Ru/C sample and (b) the sol-immobilized 5 wt % Ru/C XC72R-SI sample. Insets show the Ru($3d_{5/2}$) fitting; only the Ru fitting is showed for clarity.

(463.0 and 463.5 eV, respectively) are consistent with RuO_2, and the 0.5 eV difference between them we attribute largely to the different levels of hydration and consistent analysis of bulk hydrated and anhydrous ruthenium oxides;[27,28] this interpretation is supported by the XAFS data presented earlier.

Reduction of the supported Ru species with successive reuse cycles is evidenced by the downward shift in binding energy for both the 3p and 3d levels by ~1 eV, which is in excellent agreement with STEM results that show transformation to a more crystalline state. Interestingly, for the commercial Ru/C sample, this shift in binding energy is pronounced only after the fourth successive use, whereas it is apparent after a single use for the sol-immobilized catalyst. Although such downward shifts in energy can in principle be caused by an increase in the mean particle size, the average diameter changes revealed by STEM are too small for this magnitude of change. The final Ru(3p) energy of 462.2 eV is consistent with the formation of metallic ruthenium or RuO_x/Ru and further supported by the Ru(3d) value of 280.3 eV,[29] which is again in agreement with the STEM results.

Although the ruthenium states undergo a similar reduction, there is a marked contrast in the C(1s) and O(1s) signals between the commercial and sol-immobilized prepared Ru/C samples. For the 5 wt % Ru/C XC72R-SI samples, concomitant with the reduction of the Ru species on each successive reuse cycle is the development of prominent new C(1s) (286.7 and 289.2 eV) and O(1s) (532.5 and 533.6 eV) features (see Figures 15b and 16b). These values are consistent with the development of −C−O-containing species, such as ether or hydroxyl groups,[30] and −C═O-containing species, such as ketone, carboxylic, anhydride, and lactone groups.[30] Such binding energies would be consistent with retention of lactic acid or the formation of a poly-/cyclic-lactide at the surface.[31] These lactide species could inhibit reactivity by covering Ru active sites, and their absence in the commercial catalyst could explain why this catalyst does not deactivate. However, the increase in activity, with use, of the commercial catalyst cannot be explained by this phenomenon.

In addition, the reason that these species are not observed on the commercial catalyst must be considered. A potential explanation is that the surface species observed in the sol-immobilized catalyst is associated with a reaction with the PVA stabilizing ligand of the 5 wt % Ru/C XC72R-SI. It is known that some of the PVA will be removed from the surface of sol-immobilized catalysts on treatment with water at elevated temperatures.[32] However, only partial removal of the PVA is achieved, but this is sufficient to permit access of reactants to the catalyst surface. It is possible that the residual surface-adsorbed

DOI: 10.1021/acscatal.5b00625
ACS Catal. 2015, 5, 5047−5059

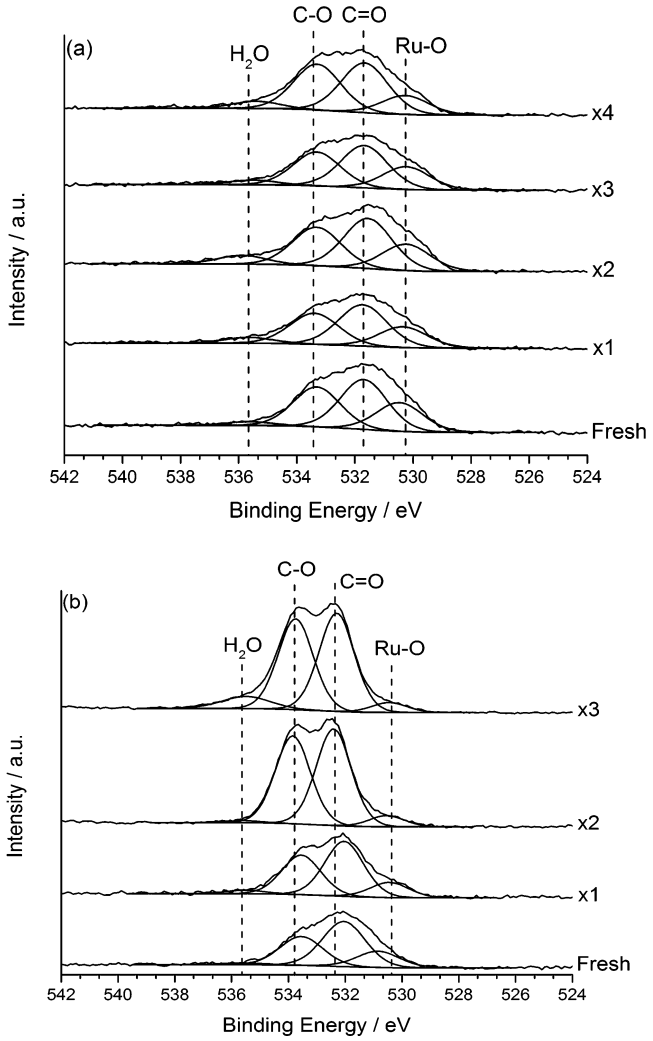

Figure 16. O(1s) core-level spectra for (a) the commercial 5 wt % Ru/C sample and (b) the sol-immobilized 5 wt % Ru/C XC72R-SI sample.

PVA can react with LA to form a surface layer, leading to deactivation. This effect would be absent in the commercial catalyst. In addition, the initial partial removal of the PVA by dissolution in the water solvent used in LA hydrogenation would explain the origin of the induction period observed with the sol-immobilized catalyst (in both the fresh and the used catalyst) because this would be expected to occur during an exposure of the catalyst to the water. These data also support our observations with respect to the time online activity data for fresh and used catalysts presented in Figure 5.

A further O(1s) species is noted at ~530 eV, whose abundance decreases with increasing catalyst use; typically, peaks around this energy are attributed to metal oxides, with the decreasing intensity supporting the reduction of ruthenium oxide to metallic Ru. Although this signal remains for both commercial and sol-immobilized samples (Figure 16a,b), this would be in agreement with RuO_x/Ru because the samples are air-handled prior to insertion in the spectrometer. The signal at 535.5 eV, which comprises ~5−8% of the total oxygen signal, can be attributed to chemisorbed water.[33] In comparison, the commercial 5 wt % Ru/C samples exhibit a similar oxygen profile, but the total concentration of oxygen and carbon functionalities is greatly reduced, as evidenced by the absence of a prominent signal ~289 eV in the C(1s)/Ru(3d) spectra (Figure 15a).

The prereduced commercial 5 wt % Ru/C catalyst (reduced in 5% H_2/Ar mixture, at 300 °C, 3 h) was also subjected to XPS analysis (before and after use). From the O(1s) and Ru(3d) spectra, reduction has a significant influence on the catalyst surface, with a marked change in the concentration and the type of oxygen species present (Supporting Information Figure S8). Moreover, reduction causes the Ru($3d_{5/2}$) signal to shift downward by 0.6 to 280.3 eV, with an equal magnitude shift for the Ru(3p) region. The final binding energy is identical to that observed for the successively used catalysts; however, the activity is reduced, and we largely attribute this to the dehydration of RuO_x, which is well-known to reduce the surface area of the oxide and, hence, have an adverse influence on the activity.[34,35] Indeed, other authors have noted a complete reduction of RuO_2 to Ru at temperatures of 477 °C[36] above the reduction temperature employed herein. This dehydration is supported by the decrease in the width of the 3p peaks, indicating the loss of a higher binding energy species and subtraction of scaled spectra confirms the presence of a peak at ~464 eV, which we attribute to $Ru(OH)_3$ (Supporting Information Figure S9).

Taken together, all the characterization data on the series of sequentially reused catalysts can be used to provide underlying reasons for the observed differing trends in catalytic behavior; namely, the observation of an induction period (with the fresh and used catalysts) and that the standard commercial sample increases in activity, whereas the catalyst prepared by sol-immobilization becomes steadily less active when compared at longer reaction times. In the case of the standard commercial catalyst, the Ru is steadily being reduced as the reaction progresses, with the particle morphology changing from raftlike structures to discrete particles and becoming progressively more active. For this material, the induction period is most likely to be due to the initial reduction coupled with morphology changes. For the sol-immobilized catalysts, the induction period is considered to be related to partial removal of the PVA stabilizing ligands coupled with initial reduction. Following the induction period with fresh catalysts, the sol-immobilized catalyst is the more active catalyst because it is in a more reduced state from the outset by virtue of the mode of catalyst preparation. Slight sintering is observed, but the particle size remains below that of the commercial catalyst. Upon use, the XPS shows that lactide species are present on the surface, and this could explain the observed partial deactivation as the reaction progresses.

CONCLUSIONS

The key features for Ru/C catalysts that need to be controlled to achieve high activity are (i) the Ru needs to be present in a reduced state and (ii) a discrete nanoparticle morphology is required. Preparation of carbon-supported Ru by sol-immobilization provides a method by which high-activity catalysts can be achieved. Comparison of the activity of this catalyst with a standard commercial Ru/C catalyst with the same metal loading showed that the sol-immobilized materials could initially achieve higher activities in relation to the commercial material; however, the sol-immobilized catalyst shows marked deactivation, which is not observed with the standard commercial catalyst. Detailed analysis shows that the effects are due to the two materials achieving rather similar morphologies and oxidation states upon use. Further work now needs to

DOI: 10.1021/acscatal.5b00625
ACS Catal. 2015, 5, 5047−5059

concentrate on stabilizing the highly dispersed catalysts that can be synthesized using the sol-immobilization method so that even higher activity can be realized and sustained.

■ ASSOCIATED CONTENT

Supporting Information

The Supporting Information is available free of charge on the ACS Publications website at DOI: 10.1021/acscatal.5b00625.

BET surface areas of catalysts, porosimetry measurements, powder X-ray diffraction analysis, temperature-programmed reduction studies, and X-ray photoelectron spectroscopy of prereduced catalysts (PDF)

■ AUTHOR INFORMATION

Corresponding Author

*E-mail: hutch@cardiff.ac.uk.

Notes

The authors declare no competing financial interest.

■ ACKNOWLEDGMENTS

We thank the ERC for funding (under ERC-2011-ADG, Grant Agreement No. 291319 ; acronym "AFTER THE GOLD-RUSH"). Funding from the EPSRC (EP/K014854/1, EP/I019693/1, EP/K014714/1) is also gratefully acknowledged. The Diamond Light Source is also thanked for provision of beam time (SP8071) and the support of their staff. The Research Complex at Harwell is also acknowledged for the use of facilities and support of their technical staff. The background for the Table of Contents and Abstract graphics is from an open access database and used with permission: https://commons.wikimedia.org/wiki/File:Grass_closeup.JPG.

■ REFERENCES

(1) Corma, A.; Iborra, S. *Chem. Rev.* **2007**, *107*, 2411−2502.
(2) Maki-Arvela, P.; Simakova, I. L.; Salmi, T.; Murzin, D. Y. *Chem. Rev.* **2014**, *114*, 1909−1971.
(3) Dasari, M. A.; Kiatsimkul, P. P.; Sutterlin, W. R.; Suppes, G. P. *Appl. Catal., A* **2005**, *281*, 225−231.
(4) Maris, E. P.; Davis, R. J. *J. Catal.* **2007**, *249*, 328−337.
(5) Miyazawa, T.; Koso, S.; Kunimori, K.; Tomishige, K. *Appl. Catal., A* **2007**, *329*, 30−35.
(6) Miyazawa, T.; Kusunoki, Y.; Kunimori, K.; Tomishige, K. *J. Catal.* **2006**, *240*, 213−221.
(7) Cortright, R. D.; Sanchez-Castillo, M.; Dumesic, J. A. *Appl. Catal., B* **2002**, *39*, 353−359.
(8) Broadbent, H. S.; Campbell, G. C.; Bartley, W. J.; Johnson, J. H. *J. Org. Chem.* **1959**, *24*, 1847−1854.
(9) Adkins, H.; Billica, H. R. *J. Am. Chem. Soc.* **1948**, *70*, 3118−3120.
(10) Zhang, Z.; Jackson, J. E.; Miller, D. J. *Appl. Catal., A* **2001**, *219*, 89−98.
(11) Chen, Y.; Miller, D. J.; Jackson, J. E. *Ind. Eng. Chem. Res.* **2007**, *46*, 3334−3340.
(12) Chheda, J. N.; Huber, G. W.; Dumesic, J. A. *Angew. Chem., Int. Ed.* **2007**, *46*, 7164−7183.
(13) Luo, G.; Yan, S.; Qiao, M.; Zhuang, J.; Fan, K. *Appl. Catal., A* **2004**, *275*, 95−102.
(14) Mao, B. W.; Cai, Z. Z.; Huang, M. Y.; Jiang, Y. Y. *Polym. Adv. Technol.* **2003**, *14*, 278−281.
(15) Yang, Q.; Zhang, J.; Zhang, L.; Fu, X.; Zheng, X.; Yuan, M.; Chen, H.; Li, R. *Catal. Commun.* **2013**, *40*, 37−41.
(16) Huang, L.; Zhu, Y.; Zheng, H.; Du, M.; Li, Y. *Appl. Catal., A* **2008**, *349*, 204−211.
(17) Yu, L.; Du, X. L.; Yuan, J.; Liu, Y. M.; Cao, Y.; He, H. Y.; Fan, K. N. *ChemSusChem* **2013**, *6*, 42−46.
(18) Primo, A.; Concepcion, P.; Corma, A. *Chem. Commun.* **2011**, *47*, 3613−3615.
(19) Newville, M. *J. Synchrotron Radiat.* **2001**, *8*, 322−324.
(20) Ravel, B.; Newville, M. *J. Synchrotron Radiat.* **2005**, *12*, 537−541.
(21) Zhang, Z.; Jackson, J. E.; Miller, D. J. *Ind. Eng. Chem. Res.* **2002**, *41*, 691−696.
(22) Jang, H.; Kim, S. H.; Lee, D.; Shim, S. E.; Baeck, S. H.; Kim, B. S.; Chang, T. S. *J. Mol. Catal. A: Chem.* **2013**, *380*, 57−60.
(23) Hengne, A. M.; Biradar, N. S.; Rode, C. V. *Catal. Lett.* **2012**, *142*, 779−787.
(24) Aika, K.; Takano, T.; Murata, S. *J. Catal.* **1992**, *136*, 126−140.
(25) McKeown, D. A.; Hagans, P. L.; Carette, L. P. L.; Russell, A. E.; Swider, K. E.; Rolison, D. R. *J. Phys. Chem. B* **1999**, *103*, 4825−4832.
(26) Altwasser, S.; Glaser, R.; Lo, A. S.; Liu, P. H.; Chao, K. J.; Weitkamp, J. *Microporous Mesoporous Mater.* **2006**, *89*, 109−122.
(27) Chan, H. Y. H.; Takoudis, C. G.; Weaver, M. J. *J. Catal.* **1997**, *172*, 336−345.
(28) Over, H. *Chem. Rev.* **2012**, *112*, 3356−3426.
(29) Shen, J. Y.; Adnot, A.; Kaliaguine, S. *Appl. Surf. Sci.* **1991**, *51*, 47−60.
(30) Chen, J. P.; Wu, S. *Langmuir* **2004**, *20*, 2233−2242.
(31) Beamson, G.; Briggs, D. High Resolution XPS of Organic Polymers − The Scienta ESCA300 Database. John Wiley & Sons Inc.: Chichester, U.K., 1992, 136−137.
(32) Lopez-Sanchez, J. A.; Dimitratos, N.; Hammond, C.; Brett, G. L.; Kesavan, L.; White, S.; Miedziak, P.; Tiruvalam, R.; Jenkins, R. L.; Carley, A. F.; Knight, D.; Kiely, C. J.; Hutchings, G. J. *Nat. Chem.* **2011**, *3*, 551−556.
(33) Laheaar, A.; Delpeux-Ouldriane; Lust, E.; Beguin, F. *J. Electrochem. Soc.* **2014**, *161*, A568−A575.
(34) Mills, A.; Davies, H. *Inorg. Chim. Acta* **1991**, *189*, 149−155.
(35) Chetty, R.; Xia, W.; Kundu, S.; Bron, M.; Reinecke, T.; Schuhmann, W.; Muhler, M. *Langmuir* **2009**, *25*, 3853−3860.
(36) Assmann, J.; Crihan, D.; Knapp, M.; Lundgren, E.; Loeffler, E.; Muhler, M.; Narkhede, V.; Over, H.; Schmid, M.; Seitsonen, A. P.; Varga, P. *Angew. Chem., Int. Ed.* **2005**, *44*, 917−920.

DOI: 10.1021/acscatal.5b00625
ACS Catal. 2015, 5, 5047−5059